# J|A|C|S

## A R T I C L E S

# Functional Nanocomposites Prepared by Self-Assembly and Polymerization of Diacetylene Surfactants and Silicic Acid

Yi Yang,[†] Yunfeng Lu,[†,‡,||] Mengcheng Lu,[†,¶] Jinman Huang,[†,#] Raid Haddad,[†]
George Xomeritakis,[†] Nanguo Liu,[†] Anthony P. Malanoski,[†] Dietmar Sturmayr,[§]
Hongyou Fan,[‡] Darryl Y. Sasaki,[‡] Roger A. Assink,[‡] John A. Shelnutt,[‡]
Frank van Swol,[†,‡] Gabriel P. Lopez,[†] Alan R. Burns,[‡] and C. Jeffrey Brinker*,[†,‡]

*Contribution from the Center for Micro-Engineered Materials and Department of Chemical and
Nuclear Engineering, The University of New Mexico, Albuquerque, New Mexico 87131,
Sandia National Laboratories, Albuquerque, New Mexico 87185, and Institute of
Inorganic Chemistry, Technical University of Vienna, A 1060 Vienna, Austria*

Received June 17, 2002 ; E-mail: cjbrink@sandia.gov

***Abstract:*** Conjugated polymer/silica nanocomposites with hexagonal, cubic, or lamellar mesoscopic order were synthesized by self-assembly using polymerizable amphiphilic diacetylene molecules as both structure-directing agents and monomers. The self-assembly procedure is rapid and incorporates the organic monomers uniformly within a highly ordered, inorganic environment. By tailoring the size of the oligo-(ethylene glycol) headgroup of the diacetylene-containing surfactant, we varied the resulting self-assembled mesophases of the composite material. The nanostructured inorganic host altered the diacetylene polymerization behavior, and the resulting nanocomposites show unique thermo-, mechano-, and solvato-chromic properties. Polymerization of the incorporated surfactants resulted in polydiacetylene (PDA)/silica nanocomposites that were optically transparent and mechanically robust. Molecular modeling and quantum calculations and $^{13}$C spin−lattice relaxation times ($T_1$) of the PDA/silica nanocomposites indicated that the surfactant monomers can be uniformly organized into precise spatial arrangements prior to polymerization. Nanoindentation and gas transport experiments showed that these nanocomposite films have increased hardness and reduced permeability as compared to pure PDA. Our work demonstrates polymerizable surfactant/silica self-assembly to be an efficient, general approach to the formation of nanostructured conjugated polymers. The nanostructured inorganic framework serves to protect, stabilize, and orient the polymer, mediate its performance, and provide sufficient mechanical and chemical stability to enable integration of conjugated polymers into devices and microsystems.

## Introduction

Natural materials such as bone and shell teach us that combining hard and soft materials in periodic architectures over multiple length scales can result in composite materials with enhanced mechanical properties such as toughness, strength, and hardness. From a materials science viewpoint, such synergistic natural composites have served as a holy grail of design and construction. However, from an engineering viewpoint, emulating natural synthetic pathways is generally either impossible or impractical, while conventional composite processing affords insufficient structural control on the meso- and microscales. Also, because of the inherent specificity of the evolutionary selection process, natural materials, like biopolymers, typically

exhibit highly developed but single functions. Here we report an efficient, evaporation-induced self-assembly procedure to prepare mechanically robust, multifunctional polymer/silica nanocomposites with hexagonal, cubic, or lamellar mesoscopic order, using *polymerizable* surfactant molecules as both structure-directing agents and monomers. Through incorporation of diacetylenic units in the hydrophobic surfactant tails, in situ polymerization enabled the formation of *conjugated polymer* (polydiacetylene) nanocomposites that have no biological counterparts.

Because of extended $\pi$-electron delocalization along their backbones, conjugated organic polymers exhibit electronic and optical properties of interest for applications ranging from light-emitting diodes to biomolecular sensors.[1] For example, in blue-colored polydiacetylene (PDA), the optical absorption blue-shifts dramatically when stress is applied to the backbone via the pendant side chains, and this thermally, mechanically, or chemically induced chromatic (blue → red) response has been explored as a colorimetric transduction scheme in a variety of chemically and physically based sensor designs.[2,3] However,

† The University of New Mexico.
‡ Sandia National Laboratories.
§ Technical University of Vienna.
|| Present address: Chemical Engineering Department, Tulane University, New Orleans, LA 70118.
¶ Present address: Intel Corp. RA1-234, 5200 NE Elam Yong Parkway, Hillsboro, OR 97124.
# Present address: Ultraphotonics, 48611 Warm Springs Blvd., Fremont, CA 94539.

(1) Charych, D.; Nagy, J.; Spevak, W.; Bednarski, M. *Science* **1993**, *261*, 585.

to improve further the optical and electronic performance of conjugated polymers and enable their integration into devices, it may be necessary to incorporate them in nanoengineered architectures that could provide alignment, control charge and energy transfer, mediate conformational changes, and impart needed mechanical and chemical stability. With respect to PDA, it is anticipated that confinement and ordering of the diacetylenic monomers within nanopores could alter their polymerization pathway vis-à-vis bulk or LB-prepared PDA. The confinement and proximity of the inorganic walls are also anticipated to influence the nature of the chromatic response and its reversibility.

More generally, it is well established that for conjugated polymers dissolved in solution or prepared as films, bends or twists of the conjugated polymer chain result in breaks in the $\pi$ conjugation, resulting in a wide range of conjugation lengths. Because the excitation energy is a strong function of conjugation length, the polymer displays an inhomogeneous distribution of physical properties such as absorption energy. Also, because defects require hopping across chains, the charge carriers (electrons or holes), while being able to move rapidly along a chain, move slowly as a whole in amorphous polymer films. Finally, when the carriers do recombine to form excitons, rapid interchain energy transfer[4] may cause the newly formed exciton to migrate to a low energy defect or trap site, quenching the physical process such as luminescence. It is therefore critical to be able to orient individual polymer chains and, in the meantime, be able to separate them beyond the effective radius of the interchain dipolar interactions that are critical in interchain energy transfer.[4] To address these problems, Tolbert and co-workers recently demonstrated control of energy transfer in a poly[2-methoxy-5-(2′-ethyl-hexyloxy-)-1,4-phenylene vinylene] (MEH-PPV)/silica nanocomposite.[4] However, this nanocomposite, prepared by MEH-PPV infiltration of a preformed, oriented hexagonal, silica mesophase, was heterogeneous, exhibiting two distinct conjugated polymer environments, viz. polymers inside and outside the hexagonally arranged pore channels of the silica particles. In general, because polymer infiltration into a preformed porous nanostructure depends on its partitioning from solvent, we expect it to be difficult to control polymer concentration, orientation, and uniformity in the corresponding nanocomposite. Further, when the nanostructure pore size is less than the radius of gyration of the solvated polymer, infiltration proceeds by a reptation mechanism in which the polymer threads itself through the pore, requiring rather long processing times at elevated temperatures.[4] In some cases, PDA being a good example, conjugated polymers are completely insoluble, making polymer infiltration through a solution phase impossible.

A related issue relevant to conjugated polymer devices is their environmental sensitivity, especially to oxygen. In that polymer/inorganic composites are considered promising candidates for barrier films for food packaging, pharmaceuticals, and corrosion inhibition, we envision that nanostructuring with relatively impermeable silicon dioxide layers or walls could reduce permeability while maintaining optical transparency. Conjugated polymer/inorganic nanocomposites therefore may serve both to
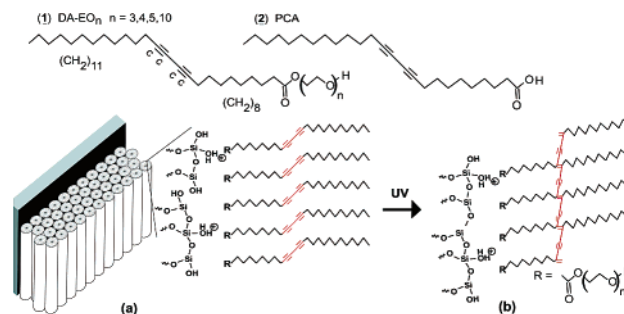


**Figure 1.** Molecular structures of DA surfactants (**1** and **2**) and polymerization of DA/silica nanocomposites. (a) Film cross section near the final stage of drying shows an oriented hexagonal mesostructure and hypothetical arrangement of DA surfactants adjacent to the cylindrically structured silicic acid framework. (b) Hypothetical structure of polymerized PDA/silica nanocomposite formed upon exposure to UV light and continued acid-catalyzed siloxane condensation (adapted from ref 7: *Nature* **2001**, *410*, 913).

enhance the performance of optoelectronic devices and to increase their chemical and mechanical stabilities.

In this paper, we discuss a hybrid organic/inorganic self-assembly process in which polymerizable amphiphilic diacetylene molecules serve as both structure-directing agents and monomers. Our self-assembly approach is rapid and prepositions both organic and inorganic precursors into highly ordered three-dimensional arrangements. In situ polymerization allows for the uniform and controlled incorporation of organic polymers within a highly ordered, inorganic environment. The resulting poly-diacetylene/silica nanocomposites are optically transparent and mechanically robust. NMR and theoretical calculations were used to model the arrangement of the surfactant molecules within the nanostructured silica host. As compared to the corresponding ordered, pure polymer films prepared by Lang-muir−Blodgett deposition,[5] nanostructuring alters the diacetylene polymerization behavior. The hybrid organic/inorganic nanocomposite materials exhibit useful thermo-, solvato-, and mechanochromic properties. They also have increased hardness and reduced gas permeability as compared to the parent polymer, which should enhance their mechanical and chemical stabilities and aid in their integration into devices.

## Experimental Section

See also Supporting Information for details.

The diacetylene (DA) surfactants (denoted **1** in Figure 1) were prepared by coupling tri-, tetra-, penta-, and decaethylene glycols with the acid chloride of 10,12-pentacosadiynoic acid (PCA) (denoted **2** in Figure 1). Precursor solutions were synthesized from tetraethyl ortho-silicate (TEOS, $Si(OC_2H_5)_4$), diacetylenic (DA-EO$_n$) surfactants (**1** with $n = 3, 4, 5, 10$, **2**, or combinations thereof), and HCl catalyst prepared in a tetrahydrofuran (THF)/water solvent. The final reactant mole ratios were 1 TEOS:31.4−84.3 THF:4.96 $H_2O$:0.013 HCl:0.06−1.41 DA surfactant.

Our approach to conjugated polymer/silica nanocomposites employs a series of oligoethylene glycol functionalized diacetylenic surfactants both as amphiphiles to direct the self-assembly of thin film silica mesophases[6] and as monomeric precursors of the conjugated polymer, PDA. Beginning with a homogeneous solution of silicic acid and surfactant prepared in a THF/water solvent with initial surfactant

(2) Cheng, Q.; Yamamoto, M.; Stevens, R. *Langmuir* **2000**, *16*, 5333.
(3) Cheng, Q.; Stevens, R. *Langmuir* **1998**, *14*, 1974.
(4) Nguyen, T.-Q.; Wu, J.; Doan, V.; Schwartz, B. J.; Tolbert, S. H. *Science* **2000**, *288*, 652.

(5) Sasaki, D. Y.; Carpick, R. W.; Burns, A. R. *J. Colloid Interface Sci.* **2000**, *229*, 490.
(6) Lu, Y. F.; Ganguli, R.; Drewien, C. A.; Anderson, M. T.; Brinker, C. J.; Gong, W.; Guo, Y.; Soyez, H.; Dunn, B.; Huang, M. H.; Zink, J. I. *Nature* **1997**, *389*, 364.

concentration $c_o$ (e.g., 0.034 M for DA-EO$_5$) much less than the critical surfactant micelle concentration cmc, we use evaporative dip-coating, spin-coating, or casting procedures to prepare thin films on silicon ⟨100⟩ or fused silica substrates.[7] During deposition, preferential evaporation of THF concentrates the depositing film in water and nonvolatile silica and surfactant species. The progressively increasing surfactant concentration drives self-assembly of diacetylene/silica micelles and their further organization into ordered liquid crystalline mesophases. Shape and concentration of the DA surfactants influence the mesophase obtained (lamellar, hexagonal, or cubic). Ultraviolet (UV) light-initiated polymerization of the DA units, accompanied by catalyst-promoted siloxane condensation, topochemically convert the colorless mesophase into the blue PDA/silica nanocomposite, preserving the highly ordered, self-assembled architecture (Figure 1).

Films were prepared by casting, spin-coating at 2000 rpm, or dip-coating at a rate of 7.6−40 cm/min in an ambient atmosphere (23−25 °C, and relative humidity between 5 and 40%). Polymerization of PDA to the blue form was done by UV exposure at 254 nm for times ranging from 30 s to 30 min. Subsequent transformation to the red form was accomplished by heating at 100 °C for times ranging from 30 s to 2 min or by exposure to solvent. A solvatochromic transition of blue PDA/silica nanocomposite films to the corresponding red films was accomplished by immersion of the blue films in the series of solvents, hexane, 2-propanol, acetone, ethanol, methanol, or dimethylformamide. Immersion times were 3 s followed by drying in nitrogen at room temperature.

## Modeling Section

**Lattice Monte Carlo Simulation.** The detailed packing and orientational information of DA monomer surfactants in cylindrical micelles was studied with a 3D three-component lattice model[8] of a water/ethanol/surfactant system. As shown previously by Larson,[9,10] this type of modeling is sufficiently coarse-grained to allow for the sampling of the spontaneous self-assembly process and the resulting 3D structures, yet sufficiently detailed to investigate the orientation of DA within the cylindrical micelle. Our lattice model represents small molecules (i.e., ethanol and water) as single sites on a simple cubic lattice with interaction potentials based on the single fluid phase diagram and employs Lorentz−Berthelot mixing rules[11] for the cross interactions.[11] The surfactant molecules are represented by a polymer chain, a collection of beads with various patterns of connectivity. Here we represent the DA molecule by a simple linear chain consisting of four hydrophilic beads ("heads", H) and four hydrophobic beads ("tails", T), or H$_4$T$_4$. NVT Monte Carlo (MC) simulations on a lattice of size 32$^3$ with periodic boundary conditions were started from a random configuration. After an initial equilibration of 10$^7$ attempted MC moves at high temperature, the temperature was dropped in five stages of 10$^7$−10$^8$ attempted MC moves, and subsequent self-assembly was followed until equilibrium was reached after approximately $3 \times 10^8$ MC moves. The initial composition was located in an area of the three-component phase diagram of H$_4$T$_4$ that our previous simulations had identified as the hexagonal phase. The description of the orientation of H$_4$T$_4$ surfactants in cylindrical micelles requires an objective analysis and was determined as

follows. First, a cluster algorithm was developed to identify all of the surfactants that make up a particular micelle. Next, we determined the principal axes of the inertia tensor of the cluster. The axis of the cylindrical micelle is determined as the inertia tensor's eigenvector with the smallest eigenvalue. We then sought to represent each H$_4$T$_4$ surfactant by a vector. Although, in principle, one could use end-to-end vectors, we decided that a superior method is to again use the inertia tensor approach, this time applied to each individual surfactant. In this fashion, we can represent each DA (i.e., H$_4$T$_4$) molecule by a unique vector that gives the molecule's orientation and is centered on the molecule's center of mass. Finally, a measure of orientational order of the H$_4$T$_4$ surfactants in the cylindrical micelle was obtained by forming the inner product of the molecule vector and the vector describing the direction of cylinder axis. We collected histograms of this inner product distribution, which is, apart from a constant, the cosine of the angle between the molecular axis and the micellar axis.

**Molecular Modeling and Quantum Calculations.** The coarse-grained lattice calculations provide valuable insight into the local packing and orientation of a collection of spontaneously self-assembled DA molecules. To assess the effects of curvature on the individual PDA oligomers, we undertook detailed molecular simulations with detailed force fields to provide realistic backbone structures whose electronic structures could then be obtained from semiempirical quantum mechanical calculations. Present computational limitations do not allow for a detailed treatment of an entire micelle of (partially) polymerized DAs. Instead, we study *single* PDA oligomers. The molecular configurations of single PDA oligomers were generated using molecular mechanics (MM) and dynamics (MD) performed with the PolyGraf software package (version 3.21) for isolated DA molecules and with Cerius$^2$ (version 4.0) for periodic calculations of molecules confined to silica pores. The particular force field used for the atomic interactions was Dreiding II with the dielectric constant set to 2.64. Partial charges in the PDA oligomer were assigned using the charge equilibration method. A MD simulation in the NVT ensemble was performed for 500 ps, during which the temperature ($T$) was fixed at 300 K. Structures were written out periodically at 0.1 ps intervals.

Semiempirical quantum calculations were performed on selected saved structures. To reduce the computational effort, we first "trimmed" the PDA structures. That is, the DA backbone of the PDA oligomers was terminated at the first methylene group of each side chain by substituting a hydrogen atom in its place. On the basis of the trimmed structures obtained from the MD simulation, we calculated UV−visible spectra of the PDA oligomers using the transition wavelengths and oscillator strengths obtained from semiempirical ZINDO/S calculations[12,13] performed using the HyperChem 5.02 software package, which provides the orbitals, energies, and transition energies and dipoles. ZINDO/S is known to give accurate spectroscopic predictions for these types of molecules when a sufficient number of HOMOs and LUMOs are included in the configuration interaction part of the calculation, as is the case here.

(7) Lu, Y. F.; Yang, Y.; Sellinger, A.; Lu, M. C.; Huang, J. M.; Fan, H. Y.; Haddad, R.; Lopez, G.; Burns, A. R.; Sasaki, D. Y.; Shelnutt, J. A.; Brinker, C. J. *Nature* **2001**, *410*, 913.

(8) Rankin, S. E.; Malanoski, A. P.; van Swol, F. *Mater. Res. Soc. Proc.* **2001**, *636*, D1.2.1.

(9) Larson, R. G. *J. Chem. Phys.* **1988**, *89*, 1642.

(10) Larson, R. G. *J. Phys. II France* **1996**, *6*, 1441.

(11) Hansen, J.-P.; McDonald, I. R. *Theory of Simple Liquids*, 2nd ed.; Academic Press: London, England, 1986.

(12) Ridley, J. E.; Zerner, M. C. *Theor. Chim. Acta* **1973**, *32*, 111.

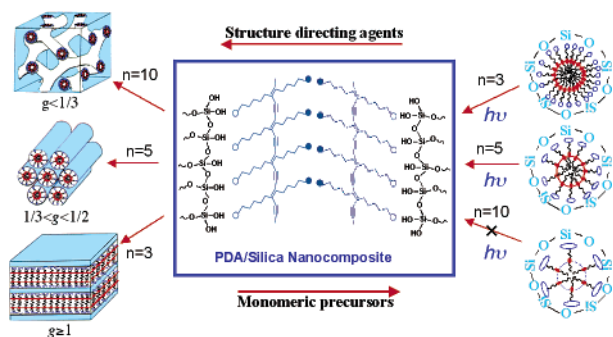(13) Bacon, A.; Zerner, M. C. *Theor. Chim. Acta* **1979**, *53*, 21.

**Figure 2.** DA surfactants serve both as amphiphiles to direct the self-assembly of the silicic acid mesostructure and as monomeric precursors of the conjugated polymer, PDA. Increasing the number, $n$, of EO subunits comprising the hydrophilic surfactant headgroup resulted in the formation of higher-curvature mesophases: lamellar ($n = 3$) → hexagonal ($n = 5$) → cubic ($n = 10$) due to a decreasing value of the surfactant packing parameter $g$.[14,15] However, larger headgroups ($n = 10$) also served as spacers, preventing polymerization of the pure DA-EO$_{10}$ surfactant. Addition of surfactants with smaller headgroups (e.g., **1** with $n = 3$ or 5, or **2**) was necessary to form PDA in the cubic system.
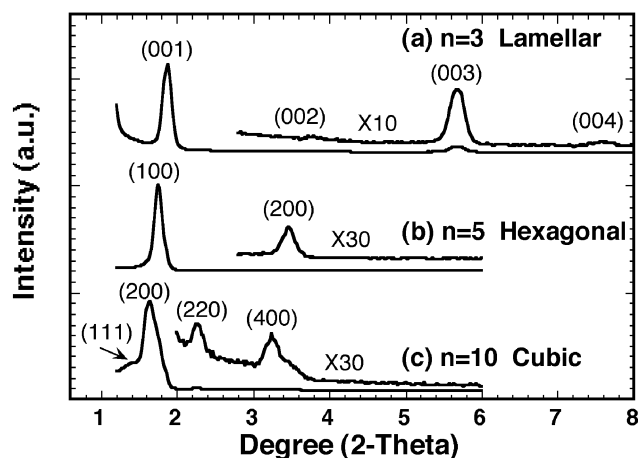


**Figure 3.** X-ray diffraction (XRD) patterns of nanocomposite thin films. (a) Film prepared using 1.86% of DA-EO$_3$ (weight % DA-EO$_3$ relative to the solution weight without surfactant) shows a lamellar mesostructure with unit cell dimension of 47 Å. (b) Film prepared with DA-EO$_5$ (2.23%) shows a hexagonal mesophase with strong (100) and (200) diffraction peaks at 50 and 25 Å, respectively. (c) Film prepared using 2.23% DA-EO$_{10}$ surfactant exhibits a face centered cubic mesophase with unit cell parameter $a = 108.2$ Å.

## Results and Discussion

**Mesostructures.** The choice of surfactant greatly influences the resultant mesostructure (Figure 2). This is evident from the XRD patterns and TEM micrographs shown in Figures 3 and 4 for nanocomposites prepared from diacetylenic surfactants with tri- ($n = 3$), penta- ($n = 5$), and decaethylene ($n = 10$) glycol headgroups. Increasing values of "$n$" increase the surfactant headgroup area $a_o$. This in turn reduces the value of the surfactant packing parameter, $g = v/a_o l$, where $v$ is the surfactant volume, and $l$ is the tail length,[14,15] favoring the formation of progressively higher curvature mesophases: lamellar ($n = 3$) → hexagonal ($n = 5$) → cubic ($n = 10$) (illustrated in Figure 2). In Figure 3a, a film prepared using 1.86% of DA-EO$_3$ (weight % DA-EO$_3$ relative to the solution weight without

(14) Israelachvili, J. N. *Intermolecular and Surface Forces*; Academic Press: San Diego, CA, 1992.
(15) Israelachvili, J. N.; Mitchell, D. J.; Ninham, B. W. *J. Chem. Soc.* **1976**, *2*, 1525.
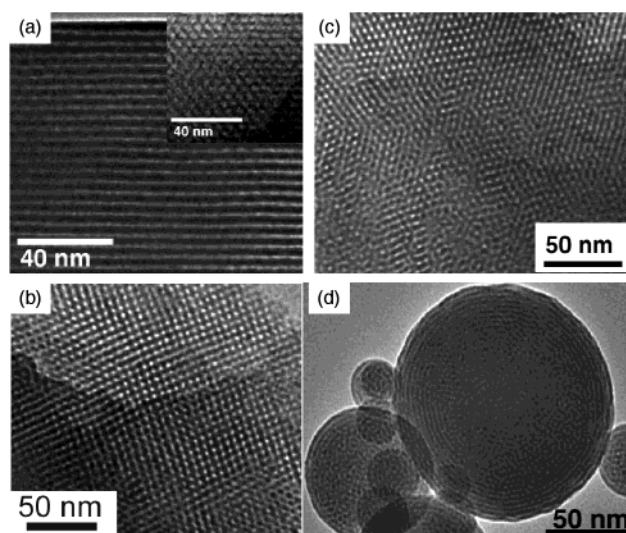
**Figure 4.** Representative TEM images of nanocomposite thin films (prepared as in Figure 3b and c) and particles (formed by a related aerosol-assisted *EISA* approach[17]). (a) [110]-Oriented hexagonally ordered nanocomposite film (inset shows [001]-orientation) prepared using 2.23% DA-EO$_5$. (b, c) Two orientations ([100] and [111]) of a cubic nanocomposite film prepared using 2.23% DA-EO$_{10}$. (d) PDA/silica nanocomposite particles prepared using an aerosol-assisted evaporation-induced self-assembly technique.

surfactant) shows a lamellar mesostructure with a (001) diffraction peak at 47 Å. The presence of higher order diffraction peaks, particularly at (003), indicates the formation of highly ordered alternating silica/PDA layers. On the other hand, the suppression of the even order peaks, such as (002) and (004), indicates comparable thicknesses[16] of the silica and polymerized DA surfactant sublayers. When 2.23% of DA-EO$_5$ was used to prepare the film, a hexagonal mesophase with the cylinder axes oriented parallel to the substrate surface resulted (Figure 3b), with strong (100) and (200) diffraction peaks at 50 and 25 Å, respectively. When a film was prepared using 2.23% DA-EO$_{10}$ surfactant, a face centered cubic mesophase was detected (Figure 3c) with unit cell parameter $a = 108.2$ Å.

In a hexagonally ordered nanocomposite film prepared using 2.23% DA-EO$_5$ surfactant, there can be seen a striped pattern (Figure 4a) that is consistent with a [110]-oriented hexagonal mesophase with repeat distance around 45 Å and regions of the corresponding hexagonally patterned mesostructure characteristic of the [001]-orientation (inset). The smaller spacing measured by TEM versus XRD (45 Å vs 50 Å, compare Figures 4a and 3b) may be due to the over-focus condition used to achieve high contrast in TEM, high vacuum, and/or electron-beam-induced shrinkage (normal to the substrate), which can occur in general for *uncalcined*, mesostructured materials. For the cubic nanocomposite film prepared using 2.23% DA-EO$_{10}$ surfactant, TEM imaging (Figure 4b) showed a highly ordered [100] orientation with unit cell parameter of 108 Å. The TEM image of the corresponding [111] orientation with repeat distance of 62 Å is shown in Figure 4c. Introduction of DA-EO$_3$, DA-EO$_5$, or PCA as cosurfactants with smaller headgroups (30−50 wt % relative to EO-DA$_{10}$) was necessary to polymerize PDA in the blue or red form within the cubic mesophase. The XRD patterns and TEM images of the cubic mesostructures were

(16) Als-Nielsen, J.; McMorrow, D. *Elements of Modern X-ray Physics*; John Wiley & Sons, Ltd.: Chichester, England, 2000.

**Table 1.** $^{13}$C NMR Spin−Lattice Relaxation Time ($T_1$) of the DA-EO$_5$ Monomer and (DA-EO$_5$)/Silica Nanocomposites

| carbon | chemical shift | $T_1$, DA-EO$_5$ | $T_1$, nanocomposites |
|---|---|---|---|
| −C≡C− | 77.1 ppm | 400 ms | 950 ms |
| −C≡C− | 66.2 ppm | 551 ms | 897 ms |
| (CH$_2$−CH$_2$−O)− | 70.6 ppm | 162 ms | 307 ms |
| CH$_2$ | 29.4 ppm | 193 ms | 305 ms |

quite comparable with and without the addition of cosurfactants (DA-EO$_3$ or DA-EO$_5$ or PCA). Figure 4d shows PDA/silica nanocomposite particles prepared using an aerosol-assisted evaporation-induced self-assembly technique.[17] The particles exhibit an ordered multilamellar exterior and a disordered wormlike mesostructured interior, consistent with a radially directed self-assembly process.[17]

From the highly ordered nanocomposite mesostructures observed by TEM, we infer that the surfactant monomers/structure-directing agents are uniformly organized into precise spatial arrangements prior to polymerization. The $^{13}$C spin−lattice relaxation time ($T_1$) is a measure of the carbon chain mobility. Table 1 shows a comparison of the $T_1$'s of different carbons species before and after being assembled into the mesopores. These carbon species exhibit well-defined resonances and provide a representative sample of the various portions of the molecule. If the monomer and silica were a simple mechanical mixture with macroscopic regions of homogeneity, then the local mobility would be unaffected, and the $T_1$ would be unchanged. However, we observed significant increases of the $T_1$'s of the monomer when it was incorporated into the silica host. The $T_1$'s of the selected carbons increased by approximately a factor of 2, indicating that the mobility of the monomer molecule has been significantly restricted in the silica nanocomposite in agreement with the gas permeability results (see below). This restriction is presumably related to the molecular ordering that has taken place in the vicinity of the rigid silica network.

Such spatial arrangements (also discussed later in the Molecular Modeling section) establish the proximity (topochemistry) of the reactive diacetylenic moieties and thus influence strongly the PDA polymerization process. This is best illustrated by comparing the polymerization behaviors, as evidenced by the blue (or red) color, of nanocomposite films prepared with different mesostructures (i.e., the hexagonal, cubic, and lamellar mesostructures shown in Figures 3 and 4) and contrasting these behaviors with those of planar self-assembled monolayer and trilayer films formed by Langmuir−Blodgett deposition of the neat DA surfactants.

**Spatial and Mesostructural Control of Polymerization Behavior.** Figure 5 shows spatial patterning of both PDA polymerization and the thermochromic blue → red transition. A nanocomposite film with a hexagonal mesostructure was formed by spin-coating a sol prepared with 2.23% of DA-EO$_5$ onto a glass substrate. A 2 min UV exposure through a mask (Figure 5a) resulted in the patterned polymerization of PDA as evident from the blue regions, the corresponding clear unpolymerized regions having been masked (Figure 5b). A subsequent heat treatment to 100 °C for 1 min resulted in a
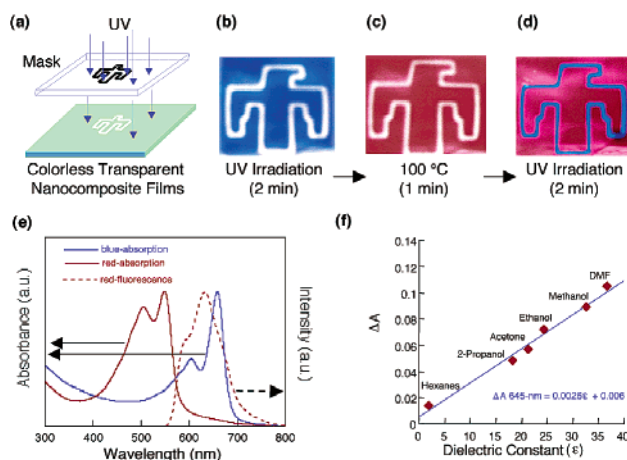
(17) Lu, Y. F.; Fan, H. Y.; Stump, A.; Ward, T. L.; Rieker, T.; Brinker, C. J. *Nature* **1999**, *398*, 223.



**Figure 5.** Patterned polymerization induced by UV irradiation and thermochromic and solvatochromic transition of hexagonal PDA/silica nanocomposite films. (a) Schematic representation of the UV patterning procedure. (b) Optical image of patterned blue/colorless film formed by UV irradiation for 2 min. (c) Patterned red/colorless film formed by heating the film in (b) to 100 °C for 1 min. (d) Patterned red/blue film formed by UV exposure of film in (c) for 2 min. (e) UV−visible spectra of the blue PDA/silica hexagonally ordered nanocomposite, the corresponding red film formed by heating at 100 °C, and the fluorescence emission spectrum of the red film (excited at 500 nm). Film formed from DA-EO$_5$. (f) Differential absorbance at 645 nm resulting from the solvatochromic transition of blue PDA/silica nanocomposite films to the corresponding red films. Without consideration of the nonpolar solvent, hexane, the regression equation is abs$_{645 nm}$ = 0.003 (dielectric constant)−0.005, correlation coefficient = 0.992 (adapted from ref 7: *Nature* **2001**, *410*, 913).

thermochromic blue → red transition (Figure 5c), the unpolymerized regions again remaining clear. A second UV exposure without the mask polymerized the clear regions, resulting in the red and blue pattern (Figure 5d). Figure 5e shows the corresponding absorption spectra of the blue and red PDA/silica films along with the photoluminescence spectrum of the red film. The blue form of PDA is not fluorescent, and this difference is of obvious importance for thermal, mechanical, and chemical sensors.

Whereas lamellar mesophases (prepared using DA-EO$_3$) exhibit polymerization and thermochromic behavior qualitatively similar to that of hexagonal mesostructures, cubic mesostructures (prepared using DA-EO$_{10}$) and Langmuir monolayers and trilayers (prepared using neat **1** with $n$ = 3, 5, or 10) remain colorless upon UV exposure and during heating (blue and red forms of other monolayer and trilayers of *polymerizable* diacetylene surfactants (e.g., PCA and PCAEA) are readily distinguishable at the air−water interface[5]). The different behaviors of lamellar and Langmuir films emphasize the importance of the nanostructured inorganic host on PDA polymerization. In both systems, the diacetylenic surfactants are organized into highly oriented planar configurations with the EO headgroups disposed toward the hydrophilic interface, either water (Langmuir films) or polysilicic acid (nanocomposites). Despite these similar organizations, we postulate that Langmuir films do not polymerize because the reactive DA moieties are spaced too far apart as indicated by the molecular areas measured at 30 mN/m in a Langmuir trough: DA-EO$_1$ = 24 Å$^2$, DA-EO$_3$ = 38 Å$^2$, DA-EO$_5$ = 46 Å$^2$. Closer spacing of the EO headgroups (and correspondingly the diacetylenic moieties) within the self-assembled nanocomposites (lamellar, hexagonal, or cubic) may be anticipated from the requirement for charge density matching at the R-EO$_{n−y}$[EO·H$_3$O$^+$]$_y$··$y$X$^-$··$w$I$^{\delta+}$ in-
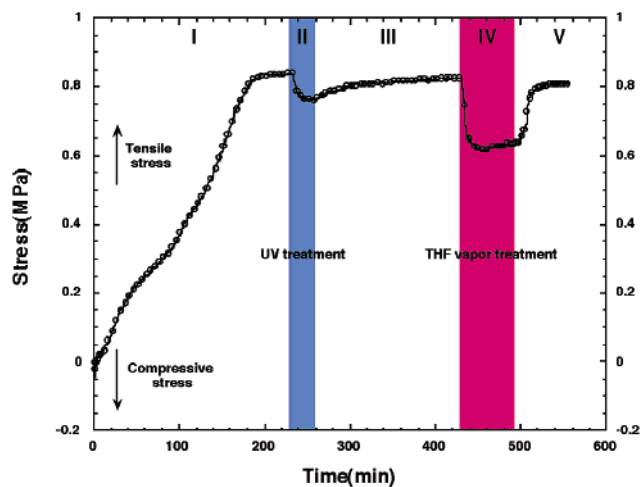
**Figure 6.** Stress development in a hexagonally ordered PDA/silica nanocomposite film upon UV irradiation and exposure to solvent (film formed from DA-EO$_4$ and stress measured using a cantilever beam technique[19,20]). The film was cast on the beam at time = 0. Region I: Silica condensation generated a tensile stress in the film. Region II: Compressive stress developed upon UV-promoted PDA polymerization (film turned blue). Region III: UV irradiation was turned off. Region IV: The film was exposed to THF vapor, resulting in the development of a compressive solvation stress and inducing the solvatochromic transition to the red fluorescent form. Region V: The film was reexposed to air, reducing the solvation stress. The net residual stress approaches a value close to that observed prior to THF exposure.

terface (where R = DA, $y \leq n$, X = Cl$^-$, I$^{\delta+}$ = the partial charge of the silica framework, and $w$ is the "concentration" of the framework needed for the charge balance) that reduces the optimal EO headgroup area $a_o$.[18]

The closer spacing of the EO headgroups is reflected in the magnitude of biaxial stress resulting from PDA polymerization measured using a cantilever beam technique.[19-21] Figure 6 shows the stress development in a hexagonally ordered PDA/ silica nanocomposite film (formed from DA-EO$_4$) upon UV irradiation and exposure to solvent. In the first stage (Region I in Figure 6), condensation of the silica framework of the nanocomposite generated a tensile stress in the film. We then observed development of compressive stress upon UV-promoted polymerization (film turns blue, Region II in Figure 6) and during the solvatochromic (Region IV in Figure 6) or thermochromic blue → red transformation, indicating a net expansion of the PDA relative to the silica host during polymerization and the chromatic transition. Qualitatively similar stress behavior was found for hexagonally ordered nanocomposites formed from DA-EO$_5$/silica and cubic films formed from mixtures of DA-EO$_3$ and DA-EO$_{10}$ as well as for other solvents that induce the solvatochromic transition.

The corresponding neat DA surfactants prepared as Langmuir monolayers do not polymerize and develop no stress upon UV irradiation. *Polymerizable* DA Langmuir monolayers and multilayers (prepared using different surfactants with smaller headgroups) contract upon polymerization, and the magnitude of this contraction is used to assess the extent of polymeriza-

tion.[22] This points to a significant difference in the organization and polymerization of the DA surfactants located at the curved silicic acid interface as compared to that on the flat water surface.

The importance of the proximity of the DA moieties on polymerization is further illustrated by our inability to polymerize DA within the cubic mesophase prepared with $n = 10$ (see Figure 3c and Figure 4b,c). The large EO$_{10}$ surfactant headgroups are necessary to direct the formation of the cubic mesophase, but they serve as spacers, preventing polymerization. Introduction of **1**, with $n = 3$ or 5, or **2** as cosurfactants with smaller headgroups (30−50 wt % relative to EO-DA$_{10}$) allows us to form cubic mesophases and to polymerize the mixed surfactant assemblies into the blue and red forms of PDA. It is expected that, due to phase separation,[23] this is not possible in Langmuir monolayers or LB films.

The polymerization of the surfactant is highly dependent upon the topological alignment of diacetylenic units within the supramolecular assembly.[24,25] Additionally, for colorimetric materials to form (especially blue colored materials), the degree of polymerization and conjugation length of the ene-yne backbone must be considerable.[26] This indicates that the micellar structures that template the silica sol−gel material must contain highly oriented, densely packed surfactants. This packing will yield facile topochemical polymerization of the diacetylene units to give colored polydiacetylene. Figure 1 illustrates a postulated lengthwise polymerization of surfactants within a cylindrical rodlike micelle to yield the blue form of PDA. Circumferential polymerization, although favored on the basis of the proximity of reactive DA moieties, would impose a high curvature on the PDA backbone due to the small pore size of the mesostructured host (2.3−3.1 nm diameter, see Figure 7).

**Physical Properties of PDA/Silica Nanocomposites.** Modulus (6.6 ± 2.00 GPa) and hardness (0.47 ± 0.2 GPa) values measured for the PDA/silica nanocomposites by nanoindentation are comparable to those of *calcined* mesoporous silica films that have been successfully integrated into microelectronic devices as low dielectric constant films[27] (Y.L. and C.J.B., unpublished). SAW-based nitrogen sorption experiments[28] show Type II sorption isotherms (Figure 7a−d), indicating that the as-deposited film and polymerized PDA/silica nanocomposite have no internal porosity accessible to N$_2$ at −196 °C,[29] indicating that the PDA completely fills the pore channels.

The corresponding permeability data for hexagonally ordered PDA/silica nanocomposites (deposited on a commercial tubular ceramic membrane support[30]) have been measured, and the results are shown in Table 2 along with values for a poly-(dodecyl methacrylate) (PDM)/silica nanocomposite film[31,32] and

(18) Monnier, A.; Schuth, F.; Huo, Q.; Kumar, D.; Margolese, D.; Maxwell, R. S.; Stucky, G. D.; Krishnamurty, M.; Petroff, P.; Firouzi, A.; M., J. *Science* **1993**, *261*, 1299.
(19) Samuel, J.; Brinker, C. J.; Frink, L. J. D.; van Swol, F. *Langmuir* **1998**, *10*, 2602.
(20) Lu, M. C. *Drying and Calcination of Sol Gel Coatings*; The University of New Mexico: Albuquerque, NM, 2001.
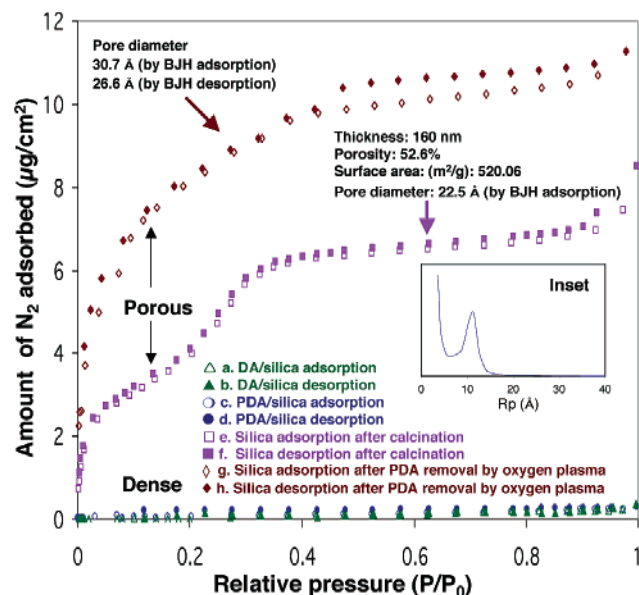(21) Stoney, G. G. *Proc. R. Soc. London* **1909**, *A82*, 172.

(22) Day, D.; Ringsdorf, H. *Polym. Sci.: Polym. Lett. Ed.* **1978**, 205.
(23) Gaines, G. L. *Insoluble Monolayers at Liquid−Gas Interfaces*; John Wiley & Sons: New York, 1966; pp 281−300.
(24) Menzel, H.; Mowery, M. D.; Cai, M.; Evans, C. E. *J. Phys. Chem. B* **1998**, *102*, 9550.
(25) Collins, M. *J. Polym. Sci., Part B: Polym. Phys.* **1988**, *26*, 367.
(26) Kuriyama, K.; Kikuchi, H.; Kajiyama, T. *Langmuir* **1988**, *4*, 6468.
(27) Lu, Y. F.; Fan, H. Y.; Doke, N.; Loy, D. A.; Assink, R. A.; LaVan, D. A.; Brinker, C. J. *J. Am. Chem. Soc.* **2000**, *122*, 5258.
(28) Frye, G. C.; Ricco, A. J.; Martin, S. J.; Brinker, C. J. *MRS Symp. Proc.* **1988**, *121*, 349−354.
(29) Gregg, S. J.; Sing, K. S. W. *Adsorption, Surface Area, and Porosity*; Academic Press Inc.: New York, 1982.
(30) Tsai, C. Y.; Tam, S. Y.; Lu, Y. F.; Brinker, C. J. *J. Membr. Sci.* **2000**, *169*, 255−268.
(31) Sellinger, A.; Weiss, P. M.; Nguyen, A.; Lu, Y. F.; Assink, R. A.; Gong, W.; Brinker, C. J. *Nature* **1998**, *394*, 256.

**Figure 7.** $N_2$ sorption isotherms of hexagonally ordered nanocomposite films acquired using a surface acoustic wave (SAW)-based technique.[28] Traces a and b: Type II adsorption−desorption isotherms of as-deposited film. Traces c and d: Type II adsorption−desorption isotherms of polymerized PDA/silica nanocomposite film. Traces e and f: Type IV adsorption−desorption isotherms of the mesoporous silica film after PDA removal by calcination at 450 °C for 3 h in air. Inset shows a pore size distribution based on adsorption data (trace e) using the BJH model.[29] Traces g and h: Type IV adsorption−desorption isotherms of the mesoporous silica film after PDA removal at room temperature using an $O_2$ plasma treatment (Fan, H., unpublished). Films were prepared using 2.23 wt % DA-EO$_5$ surfactant. The lower amount of adsorption for isotherms e and f relative to g and h reflects loss of porosity upon calcinations and differences in original film thickness.

**Table 2.** Permeabilities of PDA/Silica, PDM/Silica Nanocomposites, and Polymers

| material | temp | permeability [barrer] $[1 B = 10^{-10}$ cc cm/cm$^2$ s cmHg] | | | |
| --- | --- | --- | --- | --- | --- |
| | | He | CO$_2$ | N$_2$ | CH$_4$ |
| PDA/silica | 25 °C | 0.10 | 0.038 | 0.022 | 0.030 |
| | 100 °C | 0.11 | 0.091 | 0.029 | 0.039 |
| | 160 °C | 0.15 | 0.173 | 0.048 | 0.074 |
| PDM/silica[32] | 25°C | 0.08 | 0.12 | 0.05 | 0.067 |
| poly(decyl-acrylate)[33] | 35 °C | 54.5 | 265 | 18.4 | 55.9 |
| poly(octadecyl-acrylate)[33] | 35 °C | 7.4 | 2.96 | 0.24 | 0.53 |

two pure polyacrylate films[33] for comparison. It can be seen that the intrinsic permeability of nanostructured polymer/silica coatings is significantly lower than the values reported in the literature for pure polymers,[33] despite the very small thickness of both the PDA/silica film (56 nm) and the PDM/silica film (150 nm). The preliminary results here indeed suggest that such polymer/silica coatings have great potential for barrier properties and can be considered an alternative to presently practiced polymer-based barriers and flake films.[34] The low values of both adsorption and permeability indicate that the composite architecture may impart some degree of oxidation resistance (important for extension to other conjugated polymer nanocomposites).

To estimate the size of the pore channels in which PDA is confined, we prepared hexagonal PDA/silica nanocomposite
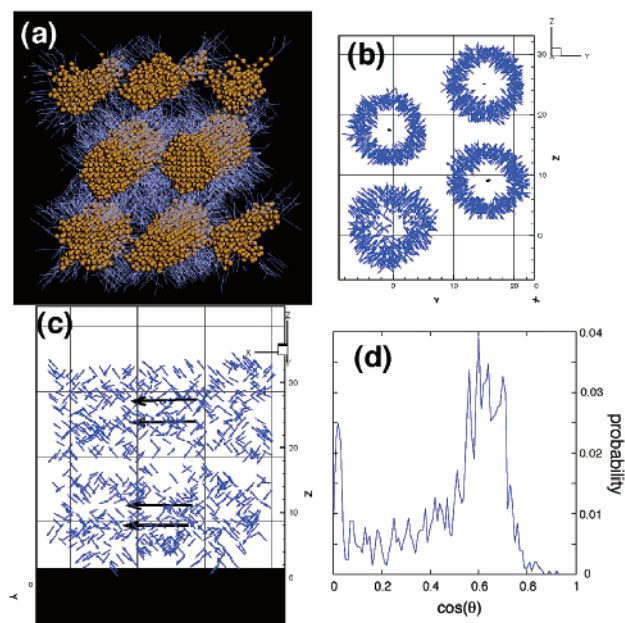
(32) Brinker, C. J.; Bond, E. M.; Chen, H.; Yang, Y.; Xomeritakis, G.; Fan, H. Y.; Yu, K.; Pardey, R. *Corrosion* **2002**, submitted.
(33) Mogri, Z.; Paul, D. R. *J. Membr. Sci.* **2000**, *175*, 253.
(34) Yang, C.; Nuxoll, E. E.; Cussler, E. L. *AIChE J.* **2001**, *47*, 295.



**Figure 8.** SA in a three-component mixture of water/ethanol and a surfactant that mimics diacetylene. (a) A space-filled rendition of the surfactant tails (yellow) and a stick representation of the headgroups (blue). (b) A head-on view, vector representation of the surfactants (blue) and the cylinder axes (black). (c) As (b) but now a side view, indicating preferential ordering. (d) Probability distribution of surfactant orientations. We plot the cosine of the angle between the surfactant axis and the cylinder axis. Note that we observe a peak near the origin and around 50°.

films on SAW devices and used an oxygen plasma treatment to remove the PDA at room temperature, thereby minimizing film shrinkage. The $N_2$ sorption isotherm of the resulting mesoporous film is shown in Figure 7g,h. It is of Type IV and exhibits a minor amount of hysteresis. BJH[29] analysis of the adsorption isotherm indicates a pore size of 3.1 nm. The hysteresis and smaller pore size measured using the desorption isotherm may be indicative of incomplete removal of the PDA, creating pore restrictions. PDA removal by calcination at 450 °C for 3 h in air resulted in a Type IV isotherm typical of highly ordered, hexagonal mesoporous silicas (Figure 7e,f). The pore diameter, 2.25 nm, calculated from the adsorption isotherm is smaller than that from TEM and XRD due to shrinkage during calcination. The inset figure shows a quite narrow pore size distribution calculated from the adsorption data (Figure 7e).

**Molecular Modeling.** The final structures obtained from the lattice MC simulation are depicted in Figure 8a, which shows hexagonally stacked cylinders. To better visualize the cylinders, we use a space-filled mode for the drawing of the tail group (yellow), use a wireframe mode for the headgroup (blue), and do not show the small molecules (water and ethanol). The headgroup faces the aqueous solution. The very tip of the headgroup is intimately intertwined with the aqueous solution. This figure clearly illustrates that, although we can easily identify the cylindrical micelles, it is impossible to assess the orientation of individual DAs from this type of representation. In Figure 8b and c, we show the results of the orientational order analysis. The black arrows indicate the direction and location of the cylinder axes, while blue unit vectors represent the orientation of some of the individual DA molecules. Each unit vector is located at the center of mass of a DA surfactant. For clarity, we do not show all of the unit vectors, but instead we have chosen those vectors that have a tilt angle close to 50°

(see below). The orientational vectors indicate that DA surfactants are tilted with respect to the cylinder axis. This is very obvious when a cylinder is viewed from the side, as in Figure 8c. A view straight down the cylinder axis (Figure 8b) reveals that the *projections* of the orientational vectors point radially toward the center. This implies that the orientational vectors tend to have no tangential component. To quantify the tilt, we calculated the inner product of the orientational vector with the direction of the cylinder axis, which gives the cosine of the tilt angle. A histogram of an ensemble average over all of the DAs is shown in Figure 8d. The probability distribution shows two peaks. One peak, near $\cos(\theta) = 0$, with the smaller integral represents a small fraction of radial alignment. The major peak, which covers the region of approximately $0.5 < \cos(\theta) < 0.8$ (i.e., $37° < \theta < 60°$), represents the majority of DAs and implies a predominant tilt angle of roughly $50°$. Note, of course, that this tilt angle can be accomplished in two ways as is obvious from Figure 7c (unit vectors tilting to the left or right). Typically, the radially aligned DAs are found where regions of different tilt meet.

Although DA surfactants organized into ellipsoidal liposomes (40 nm × 15 nm) are known to polymerize in the blue and red forms,[35] we questioned whether much more highly curved circumferential arrangements of DA surfactants such as those found from the lattice simulations (within spherical or cylindrical micelles) could polymerize with the proper ene-yne conjugation to produce colored materials. To test this, we performed a detailed simulation of cylindrically arranged DA monomers (initially energy-minimized in isolation) confined to a silica pore. The pore was constructed (using Cerius$^2$) by creating a cylindrical pore (30 Å diameter) in the center of a crystalline SiO$_2$ cylinder (63 Å long, 30 Å inner diameter, 9 Å wall thickness, cut out from a SiO$_2$ crystal structure cube of side 63 Å). Dangling Si and O atoms of the inner surface were terminated with appropriate hydrogen and hydroxyl groups. Inspired by the MC results, we investigated the packing of DA monomers within the 30 Å pores. Fifty-four DA monomers were arranged into three concentric cones of 18 monomers each with headgroups facing, but not interpenetrating, the pore wall and the tails sloping toward the pore axis. Periodic boundary conditions and the Minimum Image Convention[36] were employed in all three orthogonal directions of the cell during a 500 ps MD simulation during which the SiO$_2$ framework positions were held fixed. The MD calculations indicated that cyclic arrangements of up to 19 DA monomers around the periphery of the 30 Å diameter pore are possible.

In forming rings of polymer in pores, the ring diameter is constrained by that of the pore. As we have seen from the lattice MC simulation, the pore diameter is determined by the self-assembly of the DAs and depends on their size as well as their packing, as expressed for instance by the tilt angle. Experimental information about the pore diameter can be obtained from both N$_2$ sorption experiments and TEM studies. The PDA ring diameter will affect the "bending" between units and hence the electron conjugation and the resulting color. It is therefore of interest to determine the smallest possible ring that could still exhibit sufficient conjugation to achieve colored states. To find
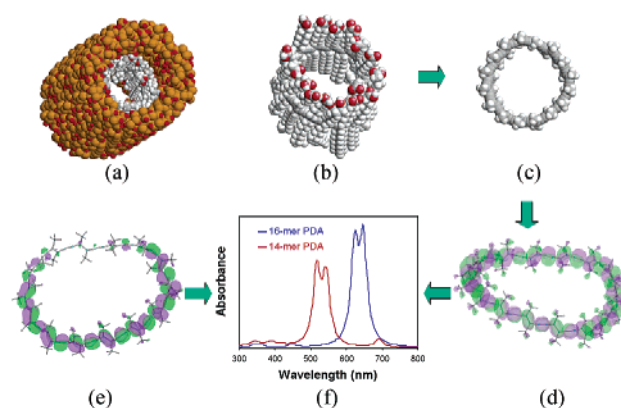
(35) Spevak, W.; Nagy, J. O.; Charych, D. H.; Schaefer, M. E.; Gilbert, J. H.; Bednarski, M. D. *J. Am. Chem. Soc.* **1993**, *115*, 1146.
(36) Allen, M. P.; Tildesley, D. J. *Computer Simulation of Liquids*; Oxford University Press: Oxford, England, 1989.

**Figure 9.** (a) Model of a 16-unit cyclic oligomer of PDA (16-mer) inside a silica pore. (b) PDA 16-mer after molecular dynamics and partial energy minimization. (c) 16-mer trimmed for quantum mechanical simulation with ZINDO/S. (d) and (e) The simulated molecular orbitals for the 16-mer and 14-mer, respectively, and (f) the associated electronic spectra (compare with Figure 5e).

the minimum number of DA units in a ring of blue form PDA, isolated PDA rings (Figure 9b) with 14 and 16 units (i.e., 14-mer and 16-mer) were constructed in an ordered conformation and energy-minimized using MM. Typically, 10 000 iterations were performed, which brings the average force down well below the typical minimization criterion of 0.1 kcal/mol. The diameters across the rings were measured: 20 Å for the 14-mer and 23 Å for the 16-mer. Electronic properties of the energy-minimized and terminated structures (Figure 9c) were obtained by applying quantum mechanical methods (Figure 9d,e). We found that an energy-minimized cyclic PDA 16-mer can exhibit absorption behavior consistent with that of the blue form of PDA. On the other hand, rings of 14 units only give rise to the red form because of the significant disruption of the conjugation (Figure 9e).

Using the results for the isolated ring with 16 units, we placed a single 16-unit ring inside the SiO$_2$ pore described above (see Figure 9a) and allowed it to undergo potential energy minimization (MM) for 5000 iterations. The resulting conformation was then analyzed with quantum mechanical methods. The simulated spectra were similar to the results for the isolated 16-unit ring, indicating that the presence of the SiO$_2$ pore walls does not significantly alter the ring conformation.

The above calculations demonstrate that a ring PDA oligomer of sufficient size can give rise to both the blue and the red form. This in no way establishes that PDA confined to nanoporous SiO$_2$ exclusively or indeed ever adopts this structure. Most likely, other nonlinear conformations, including elliptical rings or a helical structure,[37] will also allow for sufficient conjugation to exhibit both the blue and the red forms. Such nonlinear conformations are presumably rare for Langmuir monolayers and LB films, but the modeling clearly favors such structures over linear polymerization down the pore axis.

**Chromatic Transition Characteristics.** The blue PDA/silica nanocomposites exhibit solvatochromic, thermochromic, and mechanochromic properties. When contacted with the series of polar solvents, 2-propanol, acetone, ethanol, methanol, dimethylformamide, the films transform to the red, fluorescent form, and the differential absorbance at 645 nm (absorbance$_{blue}$ − absorbance$_{red}$) scales linearly with the dielectric constant of the

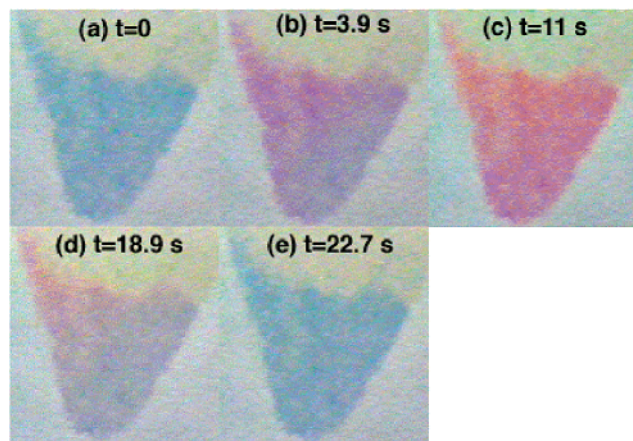(37) Frankel, D. A.; O'Brien, D. F. *J. Am. Chem. Soc.* **1991**, *113*, 7436.

**Figure 10.** Rapidly reversible thermochromic behavior of PDA/silica nanocomposite film prepared using 2.23% DA-EO$_5$ on a filter paper. (a) Blue film; (b) purple film; (c) red film; (d) purple film; (e) blue film. The film was heated using a heat gun at $t = 0$, and the heat source was withdrawn at $t = 11$ s.

solvent: $\Delta abs_{645 \text{ nm}} = 0.003$ (dielectric constant)$-0.005$, correlation coefficient $= 0.992$ (see Figure 5f), suggesting applications in sensing. We postulate that polar solvents diffuse within the polar, hydrophilic EO$_n$ pendant side chains. Accompanying solvation stresses are transferred to the PDA backbone (evidence for solvation stresses are presented in Figure 6), reducing its conjugation length, therefore inducing the blue to red transformation[38] as understood by recent molecular mechanics simulations.[39] The solvatochromic behavior shows very slow reversibility. Heating to temperatures in excess of 47°C can also cause the blue-to-red transformation. This thermochromic behavior is rapidly reversible (several seconds) and is recorded via a CCD camera using an Adobe Primere 4.0 software (see Supporting Information: a movie shows the whole thermochromic transition.) Figure 10 shows snapshots extracted from this movie that represent the different stages (colors) of a rapid reversible thermochromic transition. This may arise from hydrogen-bonding interactions[38] of the pendant side chains with the silanol moieties of the surrounding inorganic mesophase, supplying a restoring force and enabling recovery of the original side chain orientation. Mechanical abrasion of the blue nanocomposite film causes local transformation to the red fluorescent form. Thus, we envision tribochromic barrier coatings that could sense excessive mechanical damage.

## Conclusion

The use of polymerizable surfactants as both structure-directing agents and monomers in the various evaporation-driven self-assembly schemes developed recently[7,40,41] represents a general, efficient route to the formation of robust multifunctional nanocomposites. Using this approach, we fabricated PDA/silica nanocomposites, which exhibit unique thermo-, mechano-, and solvatochromic properties. The choice of surfactant greatly influences the resultant mesostructure: lamellar ($n = 3$) → hexagonal ($n = 5$) → cubic ($n = 10$). The resulting nanostructured inorganic host also altered the diacetylene polymerization behavior: the use of large EO$_{10}$ surfactant headgroups is necessary to direct the formation of the cubic mesophase, but they also serve as spacers, preventing polymerization. NMR, molecular modeling, and quantum calculation results indicated that DA surfactant monomers can be uniformly organized into precise spatial arrangements prior to polymerization, and the DA surfactants are tilted with respect to the cylinder axes in the cylindrical micelles. The calculations also demonstrated that a ring of PDA oligomer of sufficient size can give rise to both the blue and the red forms. The relations between solvatochromic properties and the dielectric constants of different solvents, the different fluorescent properties between the blue and red form PDA/silica nanocomposites, and the good mechanical properties of the nanocompite films make the PDA/silica nanocomposite films good potential candidates in sensing. The hybrid organic/inorganic nanocomposite films also have very low permeabilities as compared to that of polymer coatings and could be useful for integration of environmentally sensitive conjugated polymers and for optically transparent, self-reporting barrier materials, in general.

**Supporting Information Available:** Experimental section (PDF) and a movie showing the rapidly reversible thermochromic behavior of a PDA/silica nanocomposites film deposited on a filter paper (QT). This material is available free of charge via the Internet at http://pubs.acs.org.

JA027332J

(38) Patel, G. N.; Chance, R. R.; Witt, J. D. *J. Chem. Phys.* **1979**, *70*, 4387.
(39) Burns, A. R.; Carpick, R. W.; Sasaki, D. Y.; Shelnutt, J. A.; Haddad, R. *Tribiology Lett.* **2001**, *10*, 89.
(40) Fan, H. Y.; Lu, Y. F.; Stump, A.; Reed, S. T.; Baer, T.; Schunk, R.; Perez-Luna, V.; Lopez, G. P.; Brinker, C. J. *Nature* **2000**, *405*, 56.
(41) Brinker, C. J.; Lu, Y. F.; Sellinger, A.; Fan, H. Y. *Adv. Mater.* **1999**, *11*, 579.